


Article

A Stochastic Methodology for EV Fast-Charging Load Curve Estimation Considering the Highway Traffic and User Behavior

Leonardo Nogueira Fontoura da Silva ^{1,*}, Marcelo Bruno Capeletti ¹, Alzenira da Rosa Abaide ¹
and Luciano Lopes Pfitscher ²

¹ Graduate Program in Electrical Engineering, Federal University of Santa Maria, Santa Maria 97105-900, Rio Grande do Sul, Brazil; marcelo.capeletti@gmail.com (M.B.C.); alzenira@ufsm.br (A.d.R.A.)

² Sustainability and Energy Department, Federal University of Santa Catarina, Araranguá 88906-072, Santa Catarina, Brazil; luciano.pfitscher@ufsc.br

* Correspondence: leo.nogueirafs@gmail.com

Abstract: The theoretical impact of the electric vehicle (EV) market share growth has been widely discussed with regards to technical and socioeconomic aspects in recent years. However, the prospection of EV scenarios is a challenge, and the difficulty increases with the granularity of the study and the set of variables affected by user behavior and regional aspects. Moreover, the lack of a robust database to estimate fast-charging stations' load curves, for example, affects the quality of planning, allocation, or grid impact studies. When this problem is evaluated on highways, the challenge increases due to the reduced number of trips related to the reduced number of charger units installed and the limited EVs range, which influence user anxiety. This paper presents a methodology to estimate the highway fast-charging station operation condition, considering regional and EV user aspects. The process is based in a block of traffic simulation, considering the traffic information and highway patterns composing the matrix solution model. Also, the output block estimates charging stations' operational conditions, considering infrastructure scenarios and simulated traffic. A Monte Carlo simulation is presented to model entrance rates and charging times, considering the PDF of stochastic inputs. The results are shown for the aspects of load curve and queue length for one case study, and a sensibility study was conducted to evaluate the impact of model inputs.

Keywords: fast-charging stations; charging scenarios; queue length; Monte Carlo simulation; fast-charging load curves; EV long-distance trips



Citation: Silva, L.N.F.d.; Capeletti, M.B.; Abaide, A.d.R.; Pfitscher, L.L. A Stochastic Methodology for EV Fast-Charging Load Curve Estimation Considering the Highway Traffic and User Behavior. *Energies* **2024**, *17*, 1764. <https://doi.org/10.3390/en17071764>

Academic Editor: K. T. Chau

Received: 1 February 2024

Revised: 19 March 2024

Accepted: 23 March 2024

Published: 8 April 2024



Copyright: © 2024 by the authors. Licensee MDPI, Basel, Switzerland. This article is an open access article distributed under the terms and conditions of the Creative Commons Attribution (CC BY) license (<https://creativecommons.org/licenses/by/4.0/>).

1. Introduction

In recent years, public and private policies have been developed to improve global energy conditions, including transport market actions. Based on the reduction of Greenhouse Gas Emissions and the incentive for countries' energy autonomy, the electric vehicles (EV) market is developing [1]. Large light-duty and heavy-duty EV occurrences are already observed in China, the USA, and European countries, reflecting a global EV stock reaching 20M during 2022, between battery EVs (BEV) and plug-in hybrid EVs (PHEV) [2].

Although the new "re-fueling" paradigm was introduced by EVs, where major charging events occur at home (50–80%), the development of public charging infrastructures (PCIs) has had impact on the EV market growth [3]. Reference [4] compares the EV development and PCIs as a "chicken-or-the-egg fashion" problem, where the increase of EV stock enhances PCI implementation, which in turn impacts the EV market.

This relation is straightforward, observing the three main barriers to improving technology adherence. The first barrier, the EV battery range, is related to manufacturing technologies and traffic patterns. Second is the user anxiety range, which measures the fear level of EV users when the EV State-of-Charge (SoC) is near the minimum [5]. Finally, the charging duration time impacts the total displacement time and EV user routine. According

to [6], these conditions could be handled by increasing and distributing the PCIs and adopting fast-charging stations (FCSs) with power capacity greater than 50 kW.

Furthermore, high-power charger units reduce the charging duration time for the same charging event energy condition, aligning it with the time to re-fuel internal combustion vehicles [7]. When the PCI models are extrapolated to highways and roads, these points impact the mobility transition directly, where long-distance trips above 200 km could be concluded with energy and time safety [8,9].

However, due to the disruptive aspect of EV technologies and the development focusing on urban environments, FCSs for road or highway applications lack more specific studies about their operating conditions and business models to guarantee sustainability in this environment [10]. Behind this approach's lack is the complexity to determine traffic flow patterns and, consequently, to project the FCS load curves impacted by spatial-temporal conditions [11], mainly on first-time implementation projects.

The FCS load curves estimation improves the results of an extensive planning field. For the development of FCSs, it results in a better definition of infrastructure placing and sizing [12]. Moreover, due to the FCS power, new installations modify local power system load forecasting, and a disclosed forecasting model supports the FCS uncertainty representation [13]. Also, grid impacts, like voltage drops or feeder overload, are better estimated and anticipated for future system actions [14].

Finally, from an economic perspective, the FCS load curves evaluate the optimized relation between FCS and the local grid on energy and power capacity aspects, influencing the operation cost and, consequently, charging prices and business models [15]. The nominal power and number of charging units affect the initial costs of an FCS implementation plan. In turn, when it is evaluated from an operation view, it is related to power demand contracts according to the power available. These two parcels affect the FCS availability costs. Moreover, charging events in different day periods influence the average energy price and operational costs, mainly for time-of-use or real-time tariffs. Then, alternative load curve patterns could generate different charging prices, alternating amounts of energy consumed, or just the curve shape, influencing the relation between the user and the station and the user's own behavior. Reference [16] also highlights the impact of different tariffs' on-demand peaks, for example. When smart tariffs are adopted, the charging price must be adapted to new operational conditions.

Thus, this paper aims to develop a model to estimate the FCS hourly load curves, considering road or highway infrastructures and the spatial-temporal aspect evolving these applications. The methodology is composed of three steps. The first was modeled for user patterns recognition and determine charging duration times and FCS entry probabilities. These variables are inputs to the second step, a traffic simulation model, to evaluate the position and time that charging events will occur on the planning horizon. Finally, the third step is to sort each FCS operational routine, characterized by the charger unit uses and queue formation.

The results are FCS load and queue curves occurring in the time domain, able to identify and project regional and temporal seasonalities related to origin-destination patterns, EV market conditions, and road or highway occupancy according to hour and day type. This article presents advances in the methodology and discussion improvements from the first step of this research, considering Reference [17].

2. Literature Review

The infrastructure localization reflects different operational behaviors, comparing FCS infrastructures on highways or urban spaces. Generally, the uncertainty related to these load curves, mainly for low EV market share scenarios, is expressive. Some stochastic factors are related to the traffic dynamic due to random origin-destination (OD) pairs, highway seasonalities, user behaviors and their driving patterns, EV type, and the relation between user and EV SoC. For these reasons, FCS load curves for road or highway infrastructures have a spatial-temporal characterization [18].

Some theoretical studies define that the load curve projection must start from a traffic simulation result, mainly in the time domain, to include hourly and daily traffic variations [19]. Moreover, it is necessary to identify FCS occupancy aspects since the number of chargers is finite, resulting in a queue composition [20]. Due to the lack of user planning or anxiety range, the unbalanced use of subsequent FCSs results in queue variations [21].

The literature approaches related to PCIs and FCSs on highway load curve modeling follow two model groups. A bottom-up model is applied for scenario generation according to historical data [22]. On the other hand, in top-down models, some empirical aspects need to be modeled, characterized by probability distributions functions to estimate operational elements [23].

About bottom-up methodologies, ref. [24] estimates probability distribution functions based on local data, defining the charging start and stop time and respective SoCs. Following a Big Data application, ref. [14] proposes load curves based on battery electric vehicles (BEV) data, from charging events or V2G mode. A cluster model aggregates EV data on day types, creating a decision tree solution. Reference [25] also uses Big Data, using secure information of 105,000 trips on urban ways, defining the direct relation between traffic and charging station occupation. On the other hand, following conventional load forecasting methods, ref. [13] uses historical temporal series and fARIMA methods to decompose these series to linear, seasonal, and random components, projecting the charging station load just for 120 min ahead. Finally, on consumer behavior standardization, ref. [26] proposes a model to estimate the daily load curve considering field research about EV use patterns.

A common aspect of these references is that they are applied to urban environments. The data availability enhances these studies. Moreover, traffic variations in urban zones are smaller than in road or highway zones. Due to higher EV units circulating, seasonalities, and exogenous factors, like the traffic condition, non-urban zones must be better explored to generate confident FCS load curves.

In turn, top-down models are applied to model the FCS operation condition based on probability distribution functions (PDFs) or traffic estimations indicating entry rates on FCSs. Reference [27] estimates the load curve based on EV traffic flow PDFs, applying a queue theory M/M/s model, also considering charging duration time PDFs based on historical data. On the other hand, ref. [19] uses the same queue theory M/M/s model; however, it estimates the traffic flow on a Fluid Dynamic Traffic model based on differential equations to correlate distance and average traffic speed. Reference [12] solves a very short-term FCS load forecasting based on Monte Carlo simulations (MCS) by applying a queue theory model. Also, ref. [28] estimates regional urban FCS demand-based MCS.

Evaluating these references and following a top-down approach, this paper's methodology estimates FCS on highway load curves, observing an equilibrium between the data lack, generation, and use of traffic flow information. It reduces computational efforts, similar to [19], and increases the FCS load curve granularity to observe the spatial-temporal effects on regional optics and the variations between FCSs installed along an electric route.

Reference [17] presents the background concepts of this methodology, discussing general EV user behavior and traffic flow impacts on FCS operational conditions. Departing from these preliminary discussions and the proposal of the three-step model for FCS operational conditions, this article explores all advances considering the maturity of electric mobility conditions. It includes new models for the initial SoC and anxiety range, estimation of origin-destination patterns, and improvements in Monte Carlo processing related to the problem stochasticity. Also, new parameters relating to EV users and the charging process are proposed, increasing model capacities to represent actual behaviors and increasing this proposal's result reliability. A real case study is analyzed, and the general results and sensibilities on empirical parameters are discussed.

Paper Contributions

Based on these aspects, the paper's contributions are:

- An adaptive MCS model to estimate user behavior variables of FCS entry probability and charging duration times, considering regional OD patterns, regional influence zones, EV market, user anxiety range, and initial SoC condition.
- Improvements on the traffic flow methodology, considering [17], estimating EVs traveling on the road or highway on a time domain. Since the inputs patterns are stochastic, a discrete matrix model is proposed, with adaptive sizes according to distances and average velocities.
- An FCS operation model, based on charger unit operation matrices, where it considers the charging duration frequency distribution. Like the queue theory model, but increases this approach with recognition of hourly seasonalities, using the traffic results lastly obtained and the relation between EV user and charger technologies.
- To discuss variables affecting FCS load curves on highways, uncertainty points, and analysis about how to apply this load information in planning studies. Also, sensitivities on empirical parameter incentive discussions about secondary influences on FCS operation efficiency.

3. Methodology

The FCS on the road or highway load curves methodology is not a conventional process, mainly when load curve projections must be set on new EV environments, applying these results to expansion planning models. It occurs due to problems defining user behaviors related to the equipment (EV) and trips. In this form, besides considering the spatial-temporal characteristics and user behavior, the methodology must be highly adaptive in terms of parameters, being possible to apply to different regions and EV scenarios.

Thus, the proposed methodology is based on ten steps, divided into three blocks, corresponding to EV user behavior modeling, traffic simulation, and charging simulation. Figure 1 shows the interrelations between these steps and inputs/outputs block connections.

Firstly, the frequency distribution of charging duration time and FCS entry probabilities are processed on the EV user behavior block. The treatment of these variables is highly stochastic due to the extensive set of EV scenarios in an operational region. A Monte Carlo simulation is proposed to handle user uncertainty inputs. After, for the traffic simulation block, interest points of the road or highway are identified, looking for matrices modeling based on predictions of entries and exits at these points, distances, and average speed results in traffic flow. It is proposed as a discrete solution to the simulation horizon (T). However, the smaller the simulation step (Δt), the closer the continuity solution will be to the result. Finally, the charging simulation departs from FCS EV user entrances along the time steps, and considering local charger units, it is possible to estimate charger occupancies on the simulation horizon. Therefore, load curves and queue length are calculated assuming the temporal charger occupancy and equipment load capacity.

Some boundary conditions were applied in this article's methodology. Regarding user behavior, EV users want to recharge the energy amount for the trip conclusion, minimizing the waiting time for a charging event. The small charging duration (1 to 5 min) is valid for this article. Moreover, it was proposed that all EVs connected have a power capacity equal to the charger's nominal power. Regarding traffic simulation, highway and road senses are simulated separately, considering a regular average speed and the highway speed limit.

The following subsections will better explore these three blocks, including internal steps. Moreover, Table 1 presents the article variable list, consisting of acronyms and the meaning of each variable used in this methodology.

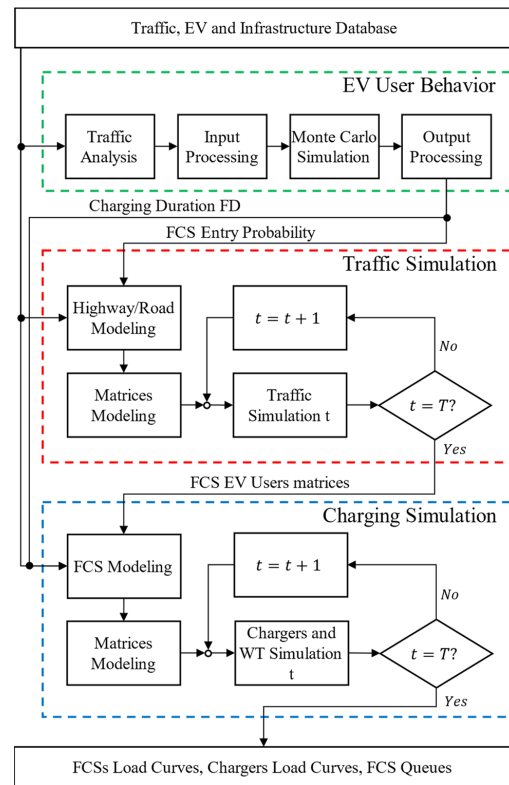


Figure 1. Methodology block diagram proposed. Three main steps are represented: user behavior, traffic simulation, and charging simulation.

Table 1. List of acronyms and variable meanings applied in this article methodology.

$F_{OD_{x,y}}$	Force between 2 points on the highway	SoC	State-of-Charge
x, y, i, j, k	Interactable variable	AR	Anxiety range
Pop_n	Normalized population of P_n	Sc_{max}	Maximum MCS scenarios
P_n	Point n on the highway	$Early_{stop}$	Maximum number of interactions without result upgrades
$d_{x,y}$	Distance between point x and point y	ϵ_{MCS}	MCS early stop accuracy index
$OD_{in_{x,y}}$	Origin index of point x observed in point y	rp_n	Highway relative position of P_n
$OD_{out_{x,y}}$	Destination index of point x observed in point y	$v_{x,y}$	Average velocity between P_x and P_y (km/h)
OD_{in_x}	Origin self-index	EV_{SP_{n-1}, P_n}	Matrix of total EV in each subpoint between P_{n-1} and P_n
OD_{out_x}	Destination self-index	SP_m	Subpoint m between two highway points
OD_{in}	Origin matrix	EV_{SP_n}	EV arriving in P_n from SP_m
OD_{out}	Destination matrix	EV_{out_P}	Matrix of total EV leaving the highway
$\gamma_{x,y}$	Empirical parameter for a better fit of OD matrix elements	$EV_{out_{P_n}}$	EV leaving the highway in P_n permanently
n	Point index	EV_{in_P}	Matrix of total EV entering the highway
N	Maximum number of highway points	$EV_{in_{P_n}}$	EV entering the highway in P_n permanently
m	Subpoint index	EV_P	Matrix of net EV number in the highway points
M	Maximum number of highways subpoints	EV_{P_n}	Net EV number in P_n
$Char_{dist_i}$	Equivalent range for charging to the scenario i (km)	t	Time step index
D_{tvd_i}	Distance traveled to Sc. i (km)	Δt	Time step length (minutes)
D_{togo_i}	Distance to go to Sc. i (km)	T	Simulation time horizon
D_{start_i}	Equivalent range considering SoC_i to Sc. i (km)	$Simul_h$	Simulation horizon (hours)
CD_i	Sc. i charging duration (minutes)	λ_P	EV entrance matrix for all FCSs along P in one highway sense
C_{unit_i}	EV Consume (kWh/km) to Sc. i	$\lambda_{FCS_{P_n}}$	Total EV entrance vector to the FCS in P_n
P_{char}	Charger Power (kW)	$C_{FCS_{P_n}}$	Binary charger matrix to the FCS in P_n
N_{char_i}	Occurrence of a charging event to Sc. i	c	Charger index
N_{next_i}	Occurrence of a postponed charging event to Sc. i	C	Total charger units of the FCS in P_n
N_{na_i}	Occurrence of a non-arrive event to Sc. i	S_c	Charger c of the FCS in P_n
N_{sc}	Total MCS simulated scenarios	Δt_{char}	Total charging event duration
F_{lim}	Flexibility index for charging events in next FCSs	δ_{FCS}	Time between two consecutive charging events
EP_{FCS}	Entrance probability of one FCS	$Load_{FCS_{P_n}}$	Load vector of the FCS in P_n
CD_{FD}	Charging duration frequency distribution	$QL_{FCS_{P_n}}$	Queue length vector of the FCS in P_n
EV_{FD}	EV type frequency distribution		

3.1. EV User Behavior

For a better comprehension of the problem treated in this paper, it is essential to define how the traffic pattern influences FCS operations. The primary key to solving this question is the EV user behavior. The user defines trip start and end points and EV battery management decisions. Therefore, modeling these aspects is fundamental for the FCS simulation.

EV user displacement patterns along a road or highway connecting n cities have some probabilities associated with departure and arrival points. This condition defines origin–destination (OD) matrices composed of pair-of-points interconnection probabilities. Some places around the world have developed specific studies about OD patterns. However, due to the methodology’s application range and low data availability premise, an OD calculation is proposed considering historical data of entrances/exits on roads or highways.

Directly, these entrance/exit data do not result in probabilities between points. Then, a concept of local influence (LI) is introduced. Figure 2 demonstrates these zones. Considering the city on P_2 , with a respective total population (Pop_2), it influences the population of P_1 and P_3 since people from towns look for services, workplaces, and leisure in big cities. This effect creates local influence zones, and displacement probabilities between P_2 and P_1 or P_3 are more significant than between P_1 and P_3 . This analysis is similar for the city on point P_{n-1} , according with the neighborhood points.

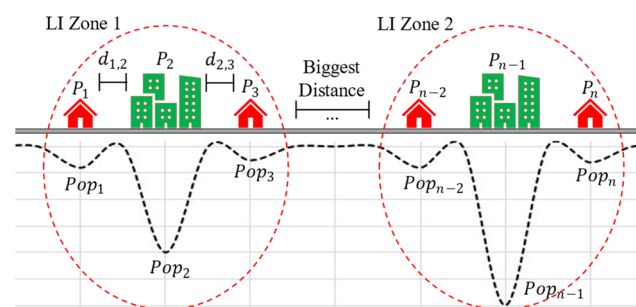


Figure 2. Interaction between local and regional influence zones, related with the population along the highway/road points.

Moreover, each pair of points has a connection distance (d), and when the distance increases, the OD probability decreases. Inspired by Newton’s theory of gravity, the population of each point and the distance between a pair x, y , generate an attraction OD force (F_{OD}), as follows:

$$F_{OD_{x,y}} = \frac{Pop_x \cdot Pop_y}{(d_{x,y})^2} \quad x \neq y, \quad (1)$$

Based on Equation (1), the connection force is directly proportional to city’s population and inversely proportional to the distance square. For example, in Figure 2, the city on P_{n-1} has the biggest population. However, by distance, the connection probability between P_2 and P_3 may be higher, due to the influence of city P_2 .

Considering this calculated force, the OD is divided into two matrices. The OD_{in} matrix, whose elements indicate the entry probabilities on point x , observing next y point, and the OD_{out} matrix, to estimate exit probabilities on the following y points, related with a previous point x .

Equations (2) and (3) show matrices element calculation. For the same point ($x = y$), both equations determine OD_{in} or OD_{out} elements proportional to own point historical average entrance or exit data. For (2), when $x < y$, the probability already estimated to $y - 1$, a point localized between the treated pair, is subtracted from the historical average entrance on x and the normalized interaction force (F_{OD}) value. For (3), the exit probability on point y reduces, when the trip starts from point x , with the distance increment between x and y , subtracting the matrix element in $y + 1$ by the historical average exit on y and the normalized F_{OD} value. In addition to highway points, x and y are matrix column and row

indexes, as seen in Equation (4). Moreover, an empirical parameter ($\gamma_{x,y}$) could be applied to adjust the far pair-of-points index, mainly above 600 km. If $\gamma_{x,y} = 1$, just the OD force is considered. Then, Equations (5) and (6), represents the OD_{in} and OD_{out} global matrices.

$$\begin{cases} OD_{in,x,y} = OD_{inx} & x = y \\ OD_{in,x,y} = \left(OD_{inx,y-1} - OD_{inx} \cdot \frac{F_{OD_{x,y}}}{\sum_{y=1}^Y F_{OD_{x,y}}} \right) \cdot \gamma_{x,y} & x < y \end{cases} \quad (2)$$

$$\begin{cases} OD_{out,x,y} = OD_{outx} & x = y \\ OD_{out,x,y} = \left(OD_{outx,y+1} - OD_{outy} \cdot \frac{F_{OD_{x,y}}}{\sum_{y=1}^Y F_{OD_{x,y}}} \right) \cdot \gamma_{x,y} & x > y \end{cases} \quad (3)$$

$$x \text{ (column)}, y \text{ (row)} = 1, 2 \dots N \quad (4)$$

$$OD_{in} = \begin{pmatrix} OD_{in1,1} & OD_{in1,2} & \dots & OD_{in1,N} \\ OD_{in2,1} & OD_{in2,2} & \dots & OD_{in2,N} \\ \dots & \dots & \dots & \dots \\ OD_{inN,1} & OD_{inN,2} & \dots & OD_{inN,N} \end{pmatrix} \quad (5)$$

$$OD_{out} = \begin{pmatrix} OD_{out1,1} & OD_{out1,2} & \dots & OD_{out1,N} \\ OD_{out2,1} & OD_{out2,2} & \dots & OD_{out2,N} \\ \dots & \dots & \dots & \dots \\ OD_{outN,1} & OD_{outN,2} & \dots & OD_{outN,N} \end{pmatrix} \quad (6)$$

In the OD_{in} matrix (Equation (5)), each line is a sub-vector for each highway point. Considering the highway senses processed separately when in Point 1 (highway extreme), the probability of entrance in this point is equal to 100%. In turn, analyzing Point 2, there are entrance probabilities on Points 1 and 2. Thus, for each FCS point processing, this sub-vector is extracted from the matrix, and the entrance highway point is randomly defined for one MCS sample according to the cumulative distribution function of this sub-vector. The same is true for the OD_{out} matrix (Equation (6)) since each line is also a sub-vector. The first line comprises all matrix terms because one EV may exit from the highway along all exits until the end of the path, considering Point 1. In this case, each point has different probabilities according to the historical data and city/town relevance.

Estimating the travel behavior characteristic, the second part of EV user behavior is characterized. Two conditions must compose the EV battery management. The first is the initial SoC, reflecting the EV range considering the first charge event before the trip. According to the distance, this value is near to 100% for highway use. Moreover, the second parameter is the anxiety range (AR). Each user has their anxiety feel, making this variable estimation difficult. In this paper, the AR is modeled as the EV SoC to stop on an FCS or at the endpoint. Based on literature reviews, the final SoC varies between 5% and 30%.

Because it is not a deterministic parameter, initial SoC and AR variables are modeled according to an equivalent probability distribution function (PDF). Since the initial SoC is near 90–100% and AR near 5–30%, a beta PDF is applied, modeling a peak near these extremes. Equation (7) presents this function based on two form parameters, α and β .

$$f_{Beta}(x, \alpha, \beta) = \frac{x^{\alpha-1} \cdot (1-x)^{\beta-1}}{\frac{\Gamma(\alpha) \cdot \Gamma(\beta)}{\Gamma(\alpha+\beta)}} \quad (7)$$

The EV type is the last variable applied to the Monte Carlo simulation. Different EV models are available, and the number will increase with the development of the EV market. Fortunately, each has its efficiency and battery size aspects, which are generally associated with price. For example, market conditions indicate that EVs with larger ranges should be more expensive due to the battery prices. Otherwise, the EV comfort and optional items also influence the cost. Thus, this variation must influence the charging necessities and duration for a highway environment.

It is proposed to identify the best-selling EVs in a study region to handle the EV types, determining the range, battery capacity, and efficiency. This ranking composes a frequency distribution and the respective cumulative distribution function, making it possible to generate one EV type for each sample.

Thus, based on these four variables, it is possible to estimate the entry probabilities of each highway FCS (EP_{FCS}) and the charging duration time (CD_{FD}). Considering stochastic aspects around input variables, a Monte Carlo simulation (MCS) model generates these outputs, according to i scenarios. Based on random input draws, considering PDFs and FDs characteristics, an origin, destination, initial SoC, AR, and EV type is associated to each scenario.

About the charging duration time, Equation (8) represents the equivalent charging distance ($Char_{dist_i}$). It is the sum of the distance traveled (D_{tvd}) and the distance to go (D_{togo}), subtracted by the capable distance with initial SoC (D_{start}). Then $Char_{dist_i}$, from i , is related to the EV consume (kW/km), and charger nominal power (P_{char}) (kW), to estimate the charging duration time (CD), as seen in Equation (9). In (9), the sum of 1 represents that the minimum connection time is 1 min. It is subtracted in Equation (11) to estimate the event occurrence.

$$Char_{dist_i} = D_{tvd_i} + D_{togo_i} - D_{start_i} \quad (8)$$

$$CD_i = \frac{Char_{dist_i} \cdot C_{unit_i} \cdot 60}{P_{char}} + 1 \quad (9)$$

The result of processing all MCS scenarios composes the charging duration time FD. Considering the entry probability, Equations (10)–(13) are applied to estimate entry probabilities (EP_{FCS}).

$$EP_{FCS} = \frac{\sum_{i=1}^{N_{sc}} N_{char_i} - \sum_{i=1}^{N_{sc}} N_{next_i}}{N_{sc} - \sum_{i=1}^{N_{sc}} N_{na_i}} \quad (10)$$

$$N_{char_i} = \begin{cases} 1 & CD_i - 1 > 0 \\ 0 & CD_i - 1 = 0 \end{cases} \quad (11)$$

$$N_{na_i} = \begin{cases} 1 & D_{tvd_i} > D_{start_i} \\ 0 & D_{tvd_i} \leq D_{start_i} \end{cases} \quad (12)$$

$$N_{next_i} = \begin{cases} 1 & N_{char_i} = 1 \text{ and } f_{cud}(x, 0, 1) \cdot N_{char_i} \leq F_{lim} \\ 0 & N_{char_i} = 0 \text{ or } f_{cud}(x, 0, 1) \cdot N_{char_i} > F_{lim} \end{cases} \quad (13)$$

Equation (10) defines the entry probability as the relation between the number of charging events (N_{char}) subtracted from possible charging events on the following FCS in the path (N_{next}), divided by the total MCS scenarios (N_{sc}), subtracted from the not available scenarios (N_{na}). Equation (11) indicates that all i scenarios with equivalent charging duration time above 0 are associated with one charging event, discounting 1 in this balance, from one-minute minimum charging duration time as defined. Equation (12) compares the distance traveled until the FCS with the initial SoC distance to determine if the EV arrives at the FCS. Finally, Equation (13) estimates how many charging events of the current FCS could occur in the following FCS installed in the path. A Limit Factor (F_{lim}) defines how many users with capacity will leave the actual FCS to recharge at the next station. If $F_{lim} = 1$, all EVs with enough range will go to the following FCS.

Algorithm 1 shows the pseudocode representation for the user behavior model, focusing on the MCS interactions aspect. Firstly, the SoC and AR PDFs, EV type (EV_{FD}), and OD matrices are modeled and introduced. The parameter Sc_{max} defines the maximum number of scenarios. $Early_{stop}$ is the number of consecutive interactions without output updates, related with an ε_{MCS} error.

Algorithm 1: Pseudocode representation for the user behavior model, returning charging duration frequency distribution and entrance probability

Input EV_{FD} , $SoC(f_{Beta}(x, \alpha, \beta))$, $AR(f_{Beta}(x, \alpha, \beta))$, OD_{in} , OD_{out}
Input Sc_{max} , $Early_{stop}$, ϵ_{MCS}
While all FCS are not processed **do**
 Initialize $CD_{FD_{j-1}} = 0$ and $EP_{FCS_{j-1}} = 0$, $j = 0$, $cont = 0$, $k = 0$
 While stopping criteria not satisfied **do**
 For $i \leftarrow 1$ to 100 **do**
 Estimate $EV_i, SoC_i, AR_i, OD_{in_i}, OD_{out_i}$, based in random numbers
 $f_{cud}(x, 0, 1)$
 Calculate $CD_i, N_{char_i}, N_{next_i}, N_{na_i}$ using (8,9,10,11,12)
 end
 $k \leftarrow k + 100$
 Estimate CD_{FD_j} with $CD_{FD_{j-1}}$ and new one hundred samples CD_i
 Estimate EP_{FCS_j} with $EP_{FCS_{j-1}}$ and new scenarios using (13)
 if $\left| \left(mean(CD_{FD_j}) - mean(CD_{FD_{j-1}}) \right) \right| < \epsilon_{SCM}$, **And**
 $\left| \left(StdDev(CD_{FD_j}) - StdDev(CD_{FD_{j-1}}) \right) \right| < \epsilon_{MCS}$, **And**
 $\left| \left(EP_{FCS_j} - EP_{FCS_{j-1}} \right) \right| < \epsilon_{SCM}$ **then**
 $cont \leftarrow cont + 1$
 else
 $cont = 0$
 end
 if $k = Sc_{max}$ **Or** $cont = Early_{stop}$ **then**
 Break
 end
 end
 Next FCS
end
Return CD_{FD} and $f_{Binomial}(x, EP_{FCS}, 1 - EP_{FCS})$ to each FCS

The number of samples (MCS scenarios) is adaptative according to the algorithm stop criteria. Each interaction comprises one hundred scenarios, and the algorithm stop occurs by two conditions: maximum scenario reached or early stop. After each interaction, the charging duration FD average, standard deviation, and FCS entrance probabilities result changes are compared with the last global result (one interaction behind). If these comparisons are behind the error (ϵ_{MCS}), it indicates low results variability, and stopping just with the $Early_{stop}$ criteria reaching. Thus, the higher the model's variable stochasticity, the higher the number of samples and interactions.

All FCSs on road or highway is independently treated, and the output is the CD_{FD} matrix for the FCSs, and a vector with binomial functions with the entry probability for all FCSs. On roads or highways with two senses, it is also processed independently, aggregating the charging duration times at the end of the EV user behavior process.

3.2. Traffic Simulation Model

Since spatial-temporal aspects impact highway or road FCS load curves, the number of EVs crossing these FCS points modifies the occupation rates and the probability of a charging event. If traffic flow projections are hardly stochastic, applications of exact models, e.g., based on differential equations, can generate confident and similar results compared with reliable approximation model. However, the second application is mathematically less complex and requires less computational effort.

Thus, a discrete solution is proposed for the traffic flow on the operation planning horizon. This model solves the traffic flow problem by minute on a regular application, updating the EVs' position at each simulation step. However, it is possible to change this granularity, where smaller steps leave the model closer to a continuous solution.

Figure 3 shows a highway/road model, considering interest points. In this case, the interest points (P_n) are towns, cities, or FCSs installed on highways. They are localized on a

relative position according to the highway origin (rp_n), separated by distances (d), and traveled at an average velocity (v).

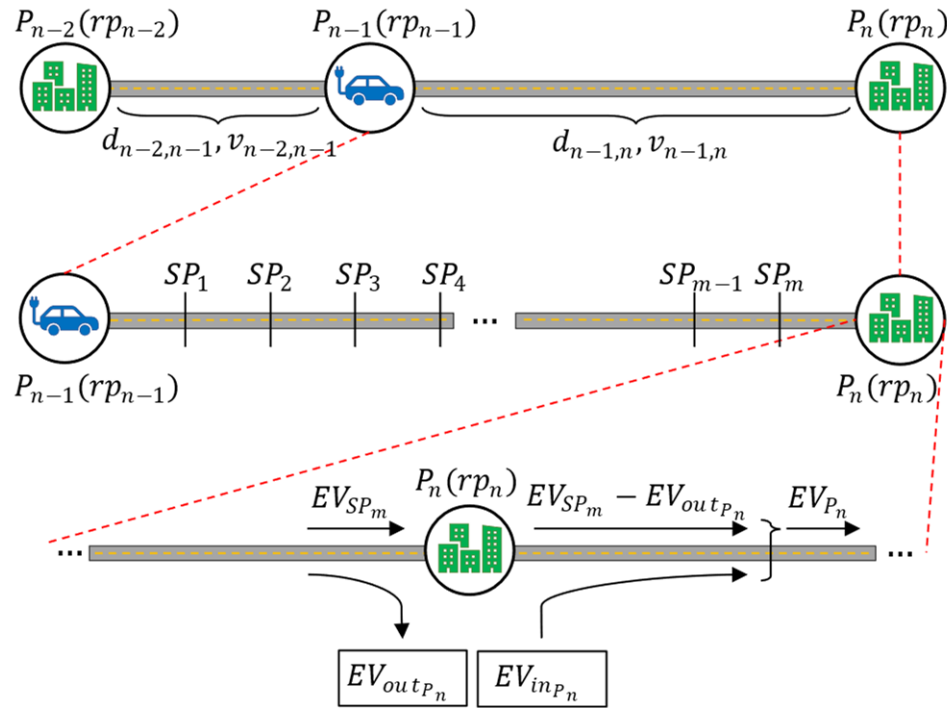


Figure 3. Highway/road model demonstrating points, subpoints, and input/output relations for each point.

In Figure 3, the interval between P_{n-1} and P_n was divided on m subpoints (SP). Still, based on this approach, it is possible to simulate the vehicle’s displacements, as will be demonstrated. Focusing on point P_n , the number of EVs departing from P_n (EV_{P_n}) is proportional to the sum of EV arriving from the last subpoint (EV_{SP_m}), with EV entering the highway (EV_{in}) subtracted from EVs exiting the highway (EV_{out}). Equation (14) presents this relation, applied to the time step t .

$$EV_{P_n}(t) = EV_{SP_m}(t) + EV_{inP_n}(t) - EV_{outP_n}(t) \tag{14}$$

Regarding Equation (14), considering a road or highway with N points, and T simulation steps (horizon), it is possible to organize this data on respective matrices. Equation (15) shows the EV_P matrix, composed by $N \cdot T$ elements, and each column is one highway point P . The matrix has T rows, based on the simulation horizon. For example, considering a daily simulation, the matrix has 1440 rows on a minute step.

Equations (16) and (17), taking the exact dimension of (15), comprise highway EV entry and exit forecasting to all points. Like highway parameters of distance and speed, this information is a model input from external data acquisition technologies like those using “digital borders” data to estimate the relation between cities/towns and the highway. Equation (18) shows matrices sizes and Equation (19) the row dimension, estimated from the simulation horizon in hours, and Δt , varying between 1 and 60.

$$EV_P = \begin{pmatrix} EV_{P_1}(t_1) & \cdots & EV_{P_N}(t_1) \\ \vdots & \ddots & \vdots \\ EV_{P_1}(T) & \cdots & EV_{P_N}(T) \end{pmatrix} \tag{15}$$

$$EV_{in_P} = \begin{pmatrix} EV_{in_{P_1}}(t_1) & \cdots & EV_{in_{P_N}}(t_1) \\ \vdots & \ddots & \vdots \\ EV_{in_{P_1}}(T) & \cdots & EV_{in_{P_N}}(T) \end{pmatrix} \tag{16}$$

$$EV_{out_P} = \begin{pmatrix} EV_{out_{P_1}}(t_1) & \cdots & EV_{out_{P_N}}(t_1) \\ \vdots & \ddots & \vdots \\ EV_{out_{P_1}}(T) & \cdots & EV_{out_{P_N}}(T) \end{pmatrix} \tag{17}$$

$$N \text{ Columns} \times T \text{ Rows} \tag{18}$$

$$T = 60 \cdot \frac{Simul_h}{\Delta t} \tag{19}$$

The last Equation (14) variable is the EV_{SP} matrix, used to estimate EVs arriving at a point P . To simulate the highway flow, matrix Equation (20) is developed. This matrix has the same T rows, however columns ($M_{n-1,n}$) are adaptative for different pair of points. It varies as Equation (22), whose columns are proportional to the integer number from the relation between distance ($d_{n-1,n}$), pair-of-points average speed ($v_{n-1,n}$), and simulation time step (Δt). For example, considering $d = 60$ km, $v = 60$ km/h, and 1 min time step, $M = 60$. However, for $v = 90$ km/h, and the same time step and distance, $M = 40$.

$$EV_{SP_{P_{n-1},P_n}} = \begin{pmatrix} EV_{SP_1}(t_1) & EV_{SP_2}(t_1) & \cdots & EV_{SP_M}(t_1) \\ EV_{SP_1}(t_2) & EV_{SP_2}(t_2) & \cdots & EV_{SP_M}(t_2) \\ \vdots & \vdots & \ddots & \vdots \\ EV_{SP_1}(T) & EV_{SP_2}(T) & \cdots & EV_{SP_M}(T) \end{pmatrix} \tag{20}$$

$$= \begin{pmatrix} EV_{P_{n-1}}(t_1 - \Delta t) & EV_{SP_1}(t_1 - \Delta t) & \cdots & EV_{SP_{M-1}}(t_1 - \Delta t) \\ EV_{P_{n-1}}(t_2 - \Delta t) & EV_{SP_1}(t_2 - \Delta t) & \cdots & EV_{SP_{M-1}}(t_2 - \Delta t) \\ \vdots & \vdots & \ddots & \vdots \\ EV_{P_{n-1}}(T - \Delta t) & EV_{SP_1}(T - \Delta t) & \cdots & EV_{SP_{M-1}}(T - \Delta t) \end{pmatrix} \tag{21}$$

$$M_{n-1,n} \text{ Columns} \times T \text{ Rows} \tag{21}$$

$$M_{n-1,n} = \text{integer} \left(\frac{60 \cdot d_{n-1,n}}{v_{n-1,n} \cdot \Delta t} \right) \tag{22}$$

Returning to the analysis of Equation (20), due to the relation between column and rows on each simulation step, the state of a determined matrix element m will be the same state of matrix element $m - 1$, in the last simulation step ($t - \Delta t$). Thereby, for $M = 60$ and $t = 0$, the EVs on SP_1 will just arrive on interest point of P_n on simulation step $t = 60$.

Finally, considering all traffic flow processed, EV_P and the binomial PDF of FCS entry probability (EP_{FCS}) are g_T function inputs to estimate the FCS EV entrance matrix (λ_P), as seen in Equation (23), representing all EV users in the simulation horizon. λ_P and EP_{FCS} have the same dimension, but only FCS points are non-zero values. All EVs on the EV_P matrix are processed separately, generating a single random number from the binomial PDF.

$$\lambda_P = g_T(EV_P, f_{Binomial}(x, EP_{FCS}, 1 - EP_{FCS})) \tag{23}$$

Algorithm 2 shows the pseudocode of the traffic simulation model. Initially, two looping structures sweep all N points of the highway/road until the simulation horizon T . During the steps, EV_{SP} is updated, resulting in the traffic flow aspect. Moreover, the EV_P matrix is also updated, considering the last submatrix element from all pair of points.

Algorithm 2: Pseudocode of the traffic simulation model, composed by the traffic flow and the EV entrance matrix calculation.

```

Input  $EV_{in_p}, EV_{out_p}, Simul_h, \Delta t, d, v$ 
Input  $f_{Binomial}(x, EP_{FCS}, 1 - EP_{FCS})$ 
Calculate  $T$  according to (19)
Generate  $EV_P$  according to (15)
Generate all  $EV_{SP_{n-1}, P_n}$  according to (20) considering results from (22)
For  $t \leftarrow 1$  to  $T$  do
     $n \leftarrow 1$ 
    While  $n < N$  do
        if  $n = 1$  then
             $EV_{SP_{n-1}, P_n}(EV_{SPM}(t)) \leftarrow 0$ 
        else if  $t = 1$  then
             $EV_{SP_{n-1}, P_n}(EV_{SPM}(t)) \leftarrow 0$ 
        else
            Update  $EV_{SP_{n-1}, P_n}$  according to (20):
             $EV_{SP_{n-1}, P_n}(EV_{SP1}(t)) \leftarrow EV_{P_{n-1}}(t - \Delta t)$ 
            For  $m \leftarrow 2$  to  $M$  do
                 $EV_{SP_{n-1}, P_n}(EV_{SPm}(t)) \leftarrow EV_{SP_{n-1}, P_n}(EV_{SP_{m-1}}(t - \Delta t))$ 
            end
            end
            Calculate  $EV_{P_n}(t)$  according to (14), considering  $EV_{SP_{n-1}, P_n}(EV_{SPm}(t))$ 
            Update  $EV_P$  according to Equation (15) considering  $EV_{P_n}(t)$ 
             $n \leftarrow n + 1$ 
        end
    end
    Estimate  $\lambda_P$  according to (23):
    For  $t \leftarrow 1$  to  $T$  do
         $n \leftarrow 1$ 
        While  $n < N$  do
            if  $EV_P(EV_{P_n}(t)) > 0$  then
                 $cont \leftarrow 0$ 
                For  $aux \leftarrow 1$  to  $EV_P(EV_{P_n}(t))$  do
                    if  $f_{Binomial}(x, EP_{FCS_{P_n}}, 1 - EP_{FCS_{P_n}}) = \text{True}$  then
                         $cont \leftarrow cont + 1$ 
                    end
                end
                 $\lambda_P(n, t) \leftarrow cont$ 
            else
                 $\lambda_P(n, t) \leftarrow 0$ 
            end
             $n \leftarrow n + 1$ 
        end
    end

```

In the second part of the Algorithm 2 pseudocode, the FCS EV entrance matrix is calculated according to function g_t . Each FCS and time step t composes one interaction of a looping structure. The algorithm estimates a true or false signal from the binomial PDF for all EVs on FCS points and increments an EV counter. After all are processed, the FCS EV user matrix is available for FCS simulation.

3.3. Fast-Charging Station Model

The FCS operation is processed on the last methodology block from Figure 1, the fast-charging station model, defining load curves and queue patterns. Firstly, the infrastructure composition is determined, mainly related to the number of chargers and their power. Since the charging duration time FD was defined considering a power parameter, this aspect must be the same for FCS processing.

Moreover, two already-processed variables are inputs of this step. A random charging duration time for each event comes from the MCS block. Otherwise, the FCS EV user matrix comprises the number of charging events for all highway FCSs modelled. Among the boundary conditions, a first-come first-serve pattern is used. Also, in this article, all EV

charging events remain on chargers' power capacity and recharge the equivalent energy to end the trip, as previously mentioned in the boundary conditions.

The FCS model is composed by a matrix solution. Initially, Equation (24) defines the sum of FCS EV user matrices, since the road or highway is composed by two senses, direct and reverse. Then, to each FCS_{P_n} , it results in a global $\lambda_{FCS_{P_n}}$ matrix. Related to FCS infrastructure, a charger's binary matrix computes time-domain charging event, as seen in Equations (25)–(27). The Equation (25) matrix has T rows, equivalent to the simulation horizon with the same time step of previous simulation steps. In addition to this, the matrix has C columns, each one corresponding an FCS charger unit. Matrix elements assume 0, for a charger waiting status on t , or 1, for an operation condition on t , as indicated by Equation (26).

$$\lambda_{FCS_{P_n}} = \lambda_{P_{direct}}(n, t_1 \rightarrow T) + \lambda_{P_{reverse}}(n, t_1 \rightarrow T) \quad (24)$$

$$C_{FCS_{P_n}} = \begin{pmatrix} S_1(t_1) & \cdots & S_C(t_1) \\ \vdots & \ddots & \vdots \\ S_1(T) & \cdots & S_C(T) \end{pmatrix} \quad (25)$$

$$S_c(t) = \begin{cases} 1 & \text{Charging Status} \\ 0 & \text{Waiting Status} \end{cases} \quad (26)$$

$$C \text{ Columns} \times T \text{ Rows} \quad (27)$$

A cumulative frequency distribution is derived from $CD_{FD_{P_n}}$ and a random number generator returns the charging duration time from one event, in minutes, as shown in Equation (28). Moreover, a parameter introduces extra charger occupation times (δ_{FCS}), representing minimum intervals between two consecutive operations (EV remotion and new EV charging start). It varies with how complex the FCS operation or user technological affinity is.

$$\Delta t_{char} = f_{CFD}(x, CD_{FD_{P_n}}) + \delta_{FCS} \quad (28)$$

After all time steps in simulation horizon processing, the FCS load curves are estimated as Equation (29). For each t time step, the sum of the product between chargers' status and chargers' power results in the time step power. Once all time steps are processed, $Load_{FCS_{P_n}}$ represents FCS load curve data. In addition, during FCS processing, for a determined time step, if all chargers had been in use and one or more EVs are waiting, they are added on the next time step. Thus, Equation (30) shows that the FCS queue matrix comes from the FCS EV user matrix treated after processing ends.

$$Load_{FCS_{P_n}} = \begin{pmatrix} \sum_{c=1}^C S_c(t_1) \cdot P_{char} & \dots \\ \vdots & \dots \\ \sum_{c=1}^C S_c(T) \cdot P_{char} \end{pmatrix} \text{ (kW)} \quad (29)$$

$$QL_{FCS_{P_n}} \propto \lambda_{FCS_{P_n}}(\text{Treated}) \quad (30)$$

This development is shown in Algorithm 3, and the road or highway FCS points are independently processed. Firstly, if an FCS is installed on P_n , the chargers' matrix, FCS EV user's matrix, and charging duration PD are initialized. Then, an external looping process of all time steps on the simulation horizon and an internal looping control the EV charging events, defining charging duration and allocating them to the chargers' matrix or adding them to the next time step. Finally, based on Equations (29) and (30), the FCS load curve and the queue length matrix are obtained and available for operation or expansion planning studies.

Algorithm 3: Pseudocode of the fast-charging station model for the load curve and queue length estimation.

```

While all points are not processed do
  if  $P_n \rightarrow \text{FCS}$  then
    Input  $C, \delta_{\text{FCS}P_n}$ 
    Generate  $C_{\text{FCS}P_n}$  according to (25)
    Calculate  $\lambda_{\text{FCS}P_n}$  using (24)
    Input  $CD_{\text{FCS}P_n}$ 
    For  $t \leftarrow 1$  to  $T$  do
       $c = 1$ 
      While  $\lambda_{\text{FCS}P_n}(t) > 0$  do
        Calculate  $\Delta t_{\text{char}}$  using (28)
        While  $C_{\text{FCS}P_n}(S_c(t)) = 1$  do
           $c \leftarrow c + 1$ 
          if  $c > C$  then
            Break
          end
        end
        if  $c \leq C$  then
           $\text{aux}t \leftarrow t$ 
          While  $\text{aux}t \leq t + \Delta t_{\text{char}}$  do
             $C_{\text{FCS}P_n}(S_c(\text{aux}t)) \leftarrow 1$ 
          end
          else
             $\lambda_{\text{FCS}P_n}(t+1) \leftarrow \lambda_{\text{FCS}P_n}(t+1) + 1$ 
          end
        end
      end
      Calculate the FCS Load Curve using (29)
      Save the FCS Queue Length like (30)
    else
      Next
    end
  end

```

4. Results and Discussion

This section develops and discusses the proposed methodology for implementing a case study, starting from base case results through sensibility analysis of model parameters. It focuses on parameters whose definitions involve empirical aspects and defines their impacts on FCS load curve results. All algorithms were implemented in Python v.3.9.12, using mainly NumPy and Pandas Libraries, and processed on an Intel Core I5 11th generation with 8 GB RAM.

4.1. Case Study

A case study from an actual highway localized in the south region of Brazil is proposed. The distance between the first and the end point of this highway is 629 km. The FCS placing is not the focus of this work, but studies like [27] consider approximately one FCS each 100 km for highway scenarios, according to EV range effects. Following these results, the case study highway starts with seven FCS. However, due to aspects such as local influences, and since this highway has two senses, more than one FCS is necessary around big cities. Therefore, 10 FCS were strategically positioned.

Moreover, thirteen heterogeneous cities exist along the highway, with different sizes, inhabitants, and economic relevance. The sum of cities and FCS points results in 23 interest points, indicated on the map of Figure 4. In this case, P5 and P15 are the main big cities, creating influence zones to the other points.

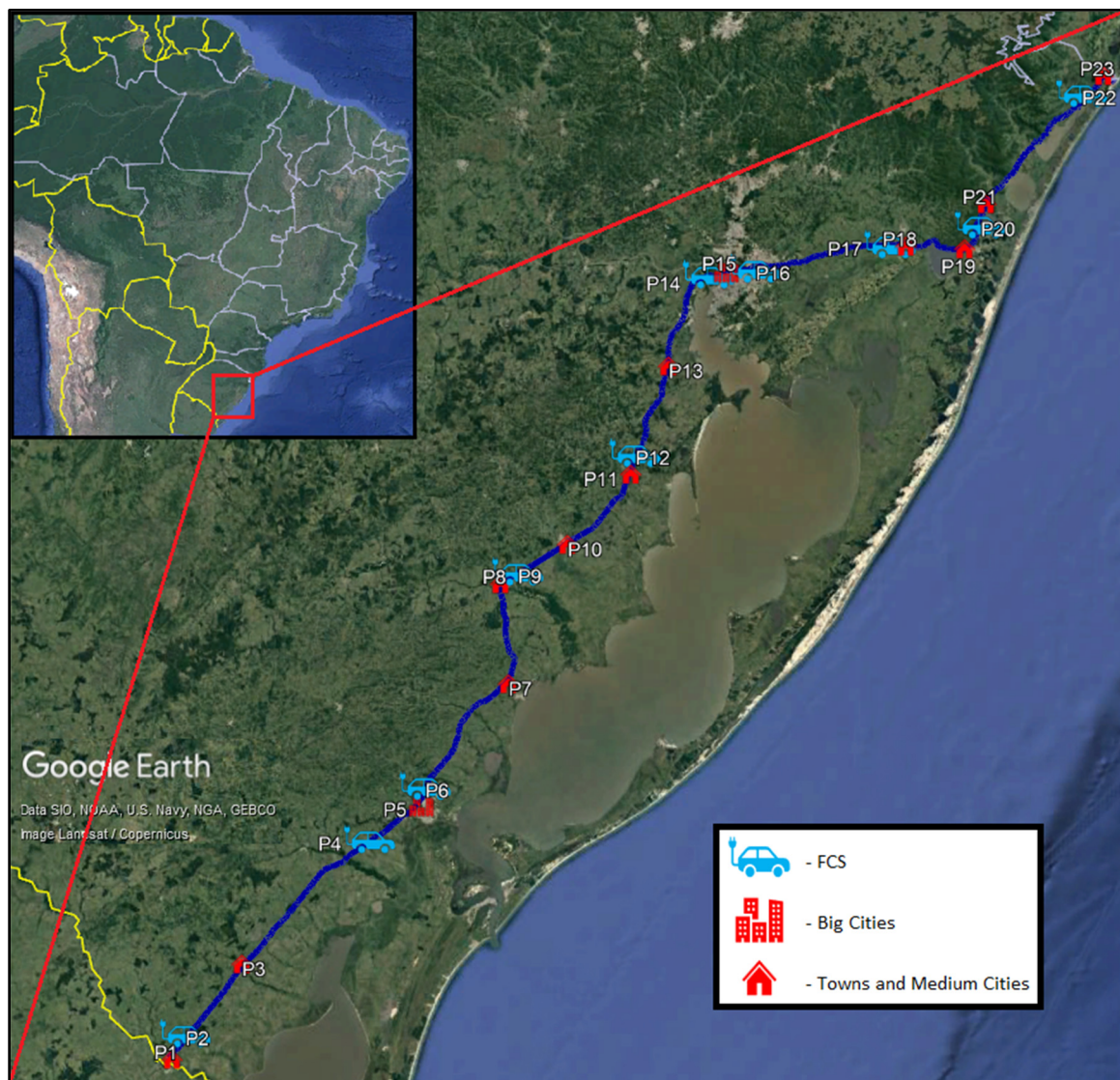


Figure 4. Case study map representation, positioning the twenty-three points modeled (thirteen cities and ten fast-charging stations).

For convention, the southern point of Figure 4 is the first, and the northern, P23, is the last. Also, the direct highway sense is from south to north (P1 to P23), and the opposite for the reverse sense. Regarding the city's entrance and exit database, information from the Transport Infrastructure National Department (TIND) was used [29], considering all 2019 data hourly.

Based on Figure 4, Table 2 shows the population, distances, and average speed for the proposed case study. About influence zones, P5 and P15, with 555,100 and 4,319,860 inhabitants, respectively, are the main points. Also, the traffic flow between P5 and P15 in both senses is expected to be higher than at highway extremes. For P19, P21, and P23, the number of inhabitants increases during the summer due to their being vacation destinations. This modifies patterns of traffic flow, influencing FCS occupation rates and, consequently, load curves and queue observations.

Table 2. Main parameters from the proposed case study.

Point	Type	Population (×1000)	Dist. Next Point (km)	Dist. Next FCS (km)	Average Speed (km/h)
P1	City	50.00	5	-	80
P2	FCS	-	40	105	80
P3	City	18.18	65	-	80
P4	FCS	-	20	25	80
P5	City	555.10	5	-	100
P6	FCS	-	58	100	100
P7	City	35.00	37	-	100
P8	City	7.28	5	-	100
P9	FCS	-	25	70	100
P10	City	47.06	35	-	100
P11	City	17.33	10	-	100
P12	FCS	-	35	73	100
P13	City	12.57	38	-	100
P14	FCS	-	5	10	100
P15	City	4319.86	5	-	100
P16	FCS	-	106	106	100
P17	FCS	-	5	40	100
P18	City	43.17	25	-	100
P19	City	135.39 ¹ /257.71 ²	10	-	100
P20	FCS	-	10	80	100
P21	City	66.26 ¹ /151.48 ²	70	-	100
P22	FCS	-	10	10	100
P23	City	39.87 ¹ /63.64 ²	-	-	100

¹ Autumn, Winter, and Spring seasons. ² Summer season.

Regarding the distance between FCS points, due to the allocation near existing services, mainly gas stations, for P2 and P16, they are located 5 km and 6 km above 100 km. However, due to EV range improvements, this is a low-impact addition. FCSs at P4 and P6, and P14 and P16, are near between them due to the influence of P5 and P15 cities, respectively. Finally, the average speed in case study simulations is 80 km/h between P1 and P5 and 100 km/h between P5 and P23, according to the highway limits.

In terms of case study traffic measures, Table 3 presents some 2019 highway entrance data information. Although it is impossible to estimate EV traffic patterns just by data, this methodology allows the composition of different market share scenarios and impacts on charging infrastructures. The base case, for example, departs from an EV market share of 1%. As seen in Table 3, the relevance of P5 and P15 is again clear. In either direct or reverse highway senses, main displacements occur between P5 and P15 and P15 and P23. For P18 and above, local maximums are observed in the reverse sense, with effect seen in the summer season. Conversely, P1 and P3 are towns with local relevance, so the traffic numbers decrease. FCSs behind P5 should have lower occupancy rates than those above P5.

Other used inputs for the MCS user behavior estimation are EV type PD, initial SoC, and anxiety range PDF. Table 4 and Figure 5 show these inputs considered in the case study. According to Brazilian regional sales, eleven EV models compose the average EV type model whose battery range indicates one to three charging events to complete the path between P1 and P23. In turn, the red curve of Figure 5 represents the anxiety range beta PDF, with $\alpha = 3$ and $\beta = 33$, and a maximum near to 6%. The initial SoC curve (black) was parameterized with $\alpha = 28$ and $\beta = 2$, and with a maximum of 96%. Both cases vary approximately 30% from the SoC extreme. These values were used for the base case, but parameter updates will be evaluated on sensibility studies.

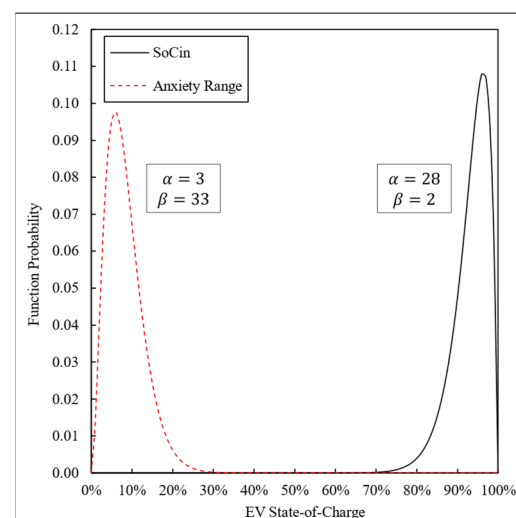
Table 3. Numbers from 2019 highway vehicle entrance used in the case study.

Point	Direct Sense		Reverse Sense	
	Veh. Average	Veh. Max	Veh. Average	Veh. Max
P1	29	159	-	-
P3	10	56	0	6
P5	390	1266	35	193
P7	23	79	3	11
P8	4	16	0	2
P10	32	105	4	15
P11	11	38	1	5
P13	8	28	0	4
P15	428	3252	368	1417
P18	4	29	40	390
P19	19	175	151	1226
P21	10	103	79	713
P23	-	-	272	1492

Table 4. Characteristics of the actual Brazilian EV market scenario.

EV	Units ¹	EV Fleet Share	Range (km)	Bat. Cap. (kWh)
Volvo XC40 RP	881	27%	300 ²	67
Porsche Taycan	495	15%	385 ²	71
Audi E-tron	459	14%	330 ²	86.5
Renault Zoe	316	10%	285 ²	52
Fiat 500e	313	9%	215 ²	37.3
Chevrolet Bolt	245	7%	300 ³	66
Jaguar I-PACE	234	7%	345 ²	84.7
JAC E-JS4	132	4%	280 ³	55
Arrizo 5E	130	4%	200 ³	53.5
Model S	61	2%	555 ²	95
Model 3	57	2%	360 ²	57.5

¹ Brazilian National Traffic Secretary Data. ² ev-DataBase. ³ Manufacturer's Information.

**Figure 5.** State-of-Charge and anxiety range curves modeled as a beta probability distribution.

4.2. Base Case Results

Based on the proposed case study, a one-year simulation horizon in an hourly time step was conducted. FCS entry probabilities and charging duration time PD have independent results for each climate season and weekdays or weekends to estimate annual seasonalities

better. Also, the base case results simulated consider a 1% EV market share (MS). Moreover, for results comprehension, FCSs were numbered according to the direct sense position, i.e., P2-FCS1, P4-FCS2, through P22-FCS10.

Figure 6 shows the FCS entry probabilities bar chart for highway senses and day types. High index variations due to traffic dynamics occur between highway senses. FCS1 direct sense results are six times greater than the same point on reverse sense. This also appears in the intermediate stations, FCS4, FCS5, FCS8, and FCS9. Since the main trip start points are P5 and P15, the FCS probabilities around these points are expected to be smaller than in the central stations, except by FCS2, the last station until P1, in the reverse sense, separated 105 km from FCS1, near to P1. This simulation generally indicates a concentration of charging events on central FCSs, according to main displacement ways.

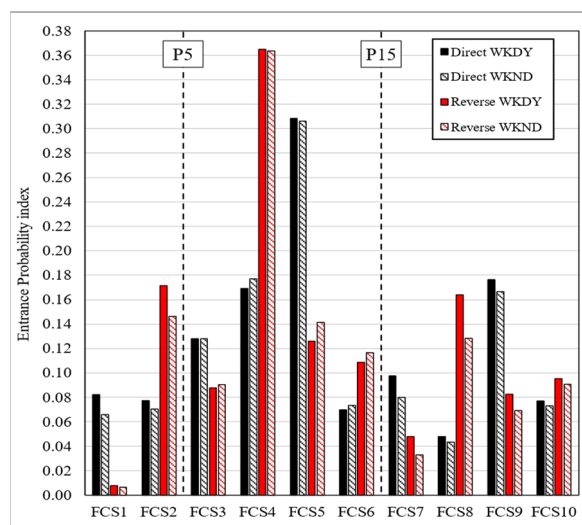


Figure 6. Bar chart for the FCS entry probability index, considering both highway senses and weekday and weekend results.

About the charging duration times, Figure 7 presents FCS4 (P9) and FCS5 (P12) curves, representing the highest entry probabilities, and FCS1 and FCS10, located on the highway extremes. Except for FCS1, the other points show maximums in the first 5 min since, in some MCS scenarios, the battery range is near the displacement distance. Also, the user-modelled interest is to charge energy to conclude the trip. For example, 5 min results in 5 kWh and approximately 25 km extra for case study EVs. FCS4, 5, and 10 also present local peaks near to 10 min. On FCS4, it is related to the reverse sense since the concentration is near 25 min in the direct sense, mainly for after P15 destinations. FCS10 presents a charging duration time local peak of 50 min due to the reverse sense conditions. Although the most negligible probabilities are for FCS1, the charging duration times occur between 20 and 35 min, mainly due to small initial SoC (70%) MCS scenarios. All FCSs were processed.

According to the second methodology block, Figure 8 shows the average and standard deviation results for the EV_p matrix, considering the highest population points, P5 and P15, in summer (a) and winter (b) for the direct sense. Initially, based on the curve average, a low EVs/hour index is expected on 1% EV MS, considering the highway traffic data. On the presented points, the average EV curves vary between 0.05 and 1.69, and a standard deviation (shadow zones) between 3.4 and 3.1 for P15 in summer and winter, respectively. The highest EV traffic concentration occurs between 6:00 and 21:00, mainly due to sunlight displacements.

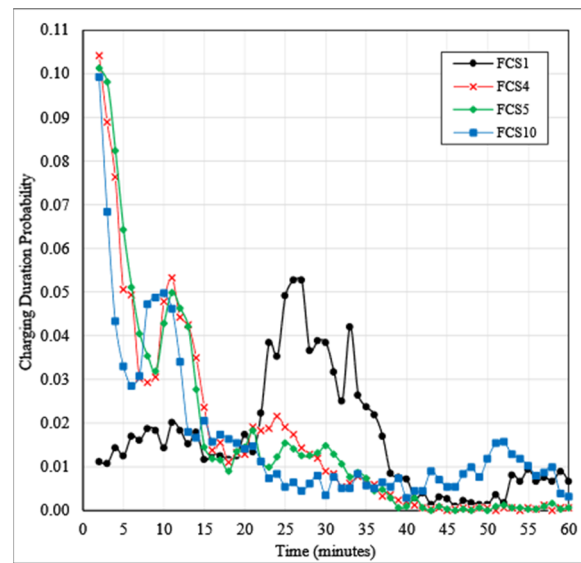


Figure 7. Charging duration PD for four modeled FCSs, FCS1 and FCS10 (borders), and FCS4 and FCS5 (highest entry probability).

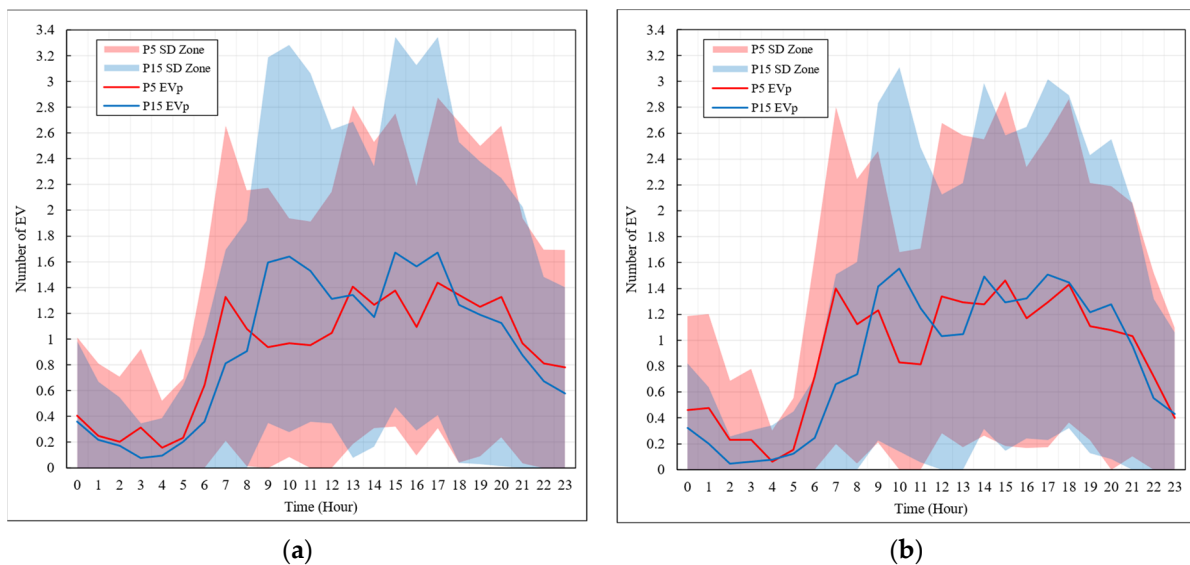


Figure 8. EV_P results for P5 and P15 (highest population), considering the direct highway sense for summer (a) and winter (b) seasons. Shaded zones represent standard deviation of the curves.

Both graphs in Figure 8 show the earlier traffic increases for P5, compared with P15, since despite local influences, P15 also has regional influence on P5. For P15, concentrations between 15:00 and 17:00 occur during summer due to the vacation condition previously explained, another seasonal effect which affects standard deviation. It has similar behaviors between graphs. However, the SD is bigger for P15, increasing the uncertainty related to the traffic data.

Traffic aspects for other highway points are generally similar, except for the highway region of P1 through P5, whose smaller traffic numbers, combined with a small market share, increase the day-to-day traffic curve variation. In terms of FCS load curves, it introduces higher uncertainty components.

Finally, the FCS operation model was processed considering the annual traffic simulation. Initially, since the FCS sizing is not an objective of this paper, one charger by FCS point was evaluated. An empirical study was conducted to expand this conclusion and found a maximum of 10 EVs waiting for charging criteria on quantile 0.99. That is, during

99% of the year, the queue must be smaller than 10. Thus, for a 1% EV MS, one 60 kW charger was sufficient, except FCS4, which has the highest entry probability, requiring two charger units.

Table 5 shows the total, maximum, and minimum consumption months for the FCS annual energy consumption simulated. Since the occupancy rates increase, there are direct relations between the FCS entry probabilities and the total FCS energy consumed. FCS4 and FCS5 presented the highest values, 274.58 MWh and 185.82 MWh, respectively.

Table 5. Energy consumed for all FCS simulated in the base case.

FCS	2019 FCS	Max. Cons.		Min. Cons.	
	Energy (MWh)	Month	MWh	Veh. Max	MWh
FCS1	10.65	January	1.48	June	0.54
FCS2	97.09	January	9.87	April	6.77
FCS3	76.19	January	8.78	May	4.89
FCS4	274.58	January	29.33	June	20.13
FCS5	185.82	January	20.99	April	13.22
FCS6	100.20	January	12.84	June	5.91
FCS7	162.62	June	14.82	May	12.02
FCS8	147.33	January	15.17	September	10.65
FCS9	197.05	December	19.09	September	13.50
FCS10	104.72	January	11.05	November	7.36

However, variations such as charging time and traffic pattern conditions influence the energy sold besides the entry probabilities. Comparing FCS8 and FCS9, although similar in probabilities in Figure 6, the second sold 34% more energy. In general, all EVs at FCS9 will end the trip with a distance travelled of 241 km, next to the EV type average range, increasing the charging energy necessities at this point.

Also, the spatial position is relevant; e.g., for FCS1, the lowest energy result is 7.5 times smaller than the second smaller energy result. At this point, the entry probabilities and the traffic flow are small. Regarding the consumption variation, the most significant values occur in the Brazilian summer months, December and January. Moreover, this result justifies the seasonality modelling since the energy consumption relation between maximum and minimum comes from 1.23 for FCS7 to 2.17 for FCS6.

Furthermore, regarding paper aims, Figure 9 shows the average daily load curves for all FCS on summer (a) and winter (b) days. For both graphs, the curves with high peaks are at FCS4, reaching approximately 60 kW. The lowest result is for FCS1, whose average maximum varies between 3 kW and 4 kW, denoting low occupancy rates. Moreover, for all FCSs between P1 and P15 (FCS1–FCS6), the average hourly loads increase during the day until 21:00 due to the reverse sense flow after 15:00. The charging times on this highway path in a reverse sense are longer than on direct one. This explains the winter FCS4 peak near 19:00.

In a global analysis, the FCS load curves follow regional traffic patterns. However, with representative queue occurrences, the load behavior stays near the maximum power for specific days despite a momentaneous traffic flow reduction. Finally, observing Figure 9 curves, occupancy rates and EV market share affect load curve uncertainty. The FCS1 load curve is deeply stochastic since it is exposed to some periods without any charging events. Then, thinking about load curve applications in planning studies, the condition introduces complex uncertainty components for the results.

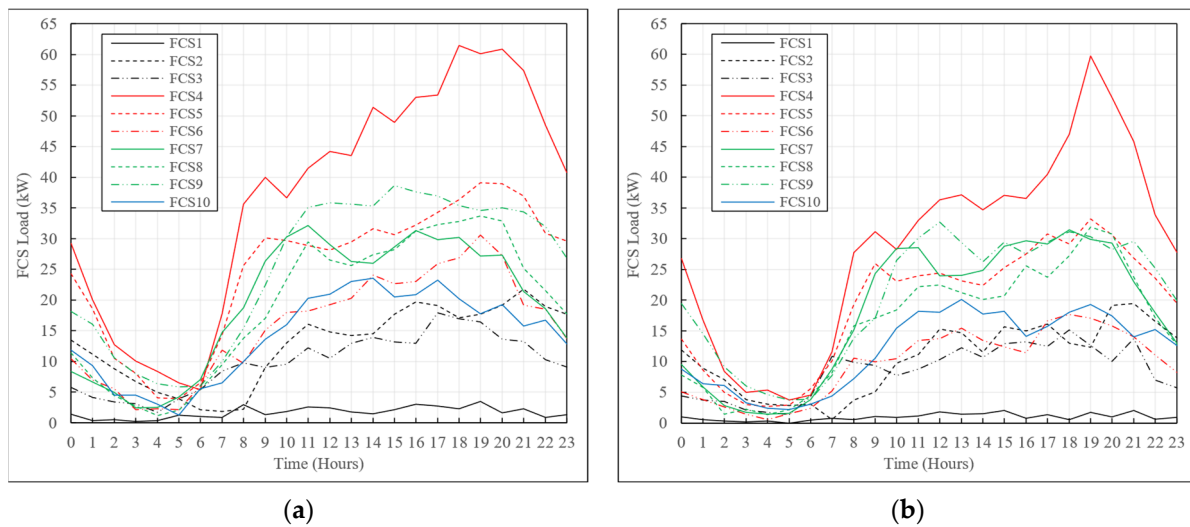


Figure 9. FCS average load curve for all simulated FCS points in summer (a) and winter (b) seasons.

4.3. Sensibilities Analysis

Despite the limited available historical data, reducing empirical influences was one aspect of this methodology proposal. However, some strategic decision-making is essential and could support applications such as load curve projections for future scenario variations. This section presents some sensibilities analysis related to these empirical parameters.

First, about the EV market share conditions. As estimated on the base case, the EV MS and the FCS entry probabilities affect occupancy rates. Thereby, as EV MS increases, current FCS infrastructure will saturate in terms of queues, making it an insoluble problem. Three MS variations were proposed: 0.1%, 1%, and 5%. Table 6 shows charger units defined for each FCS, and Figure 10 comprises a bar chart from queue quantiles 0.9 and 0.99.

Table 6. Charger units defined for each FCS point and market share scenarios.

Station	Point	0.10% EV MS	1.00% EV MS	5.00% EV MS
FCS1	P2	1 (60 kW)	1 (60 kW)	1 (60 kW)
FCS2	P4	1 (60 kW)	1 (60 kW)	1 (60 kW)
FCS3	P6	1 (60 kW)	1 (60 kW)	3 (180 kW)
FCS4	P9	1 (60 kW)	2 (120 kW)	6 (360 kW)
FCS5	P12	1 (60 kW)	1 (60 kW)	5 (300 kW)
FCS6	P14	1 (60 kW)	1 (60 kW)	4 (240 kW)
FCS7	P16	1 (60 kW)	1 (60 kW)	4 (240 kW)
FCS8	P17	1 (60 kW)	1 (60 kW)	5 (300 kW)
FCS9	P20	1 (60 kW)	1 (60 kW)	4 (240 kW)
FCS10	P22	1 (60 kW)	1 (60 kW)	3 (180 kW)

As seen in Table 6, in the 0.1% MS scenario, all FCSs have one charger. This also occurred for 1% MS, except FCS4, which considers two units. However, in the 5% MS scenario, only FCS1 and FCS2 remain with one charger, respecting the Q0.99 queue rule. For FCS4, it is necessary to have six chargers, and for FCS5 and FCS8, five units of 60 kW. Another conclusion is that FCS8 has smaller energy consumption than FCS9, on 1% MS, but needs more chargers for the 5% scenario, indicating a more significant number of short-time charging events. Observing Figure 10, for 1% MS, FCS9 will receive the next investment in a charger due to a limit queue on Q0.99, and the same for the 5% MS condition, together with FCS7. FCS1 did not process any queue on Q0.99 for 5% MS, becoming the last expansion point.

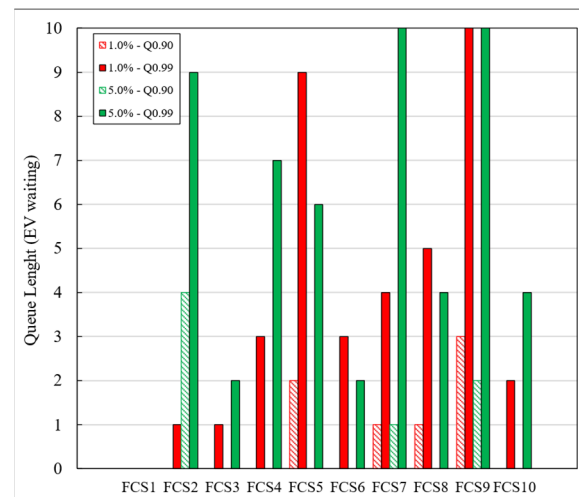


Figure 10. Bar chart of quantiles Q0.90 and Q0.99 to all FCS simulated, considering different EV market shares.

Figure 11 shows the FCS4 average load curves, varying the EV MS scenarios. Comparing load curves maximum, for 0.1%, it reaches a maximum average of 10 kW, increasing to 60 kW and 220 kW approximately, for 5%. Moreover, the relation between maximum and minimum increases with MS variation, following traffic curve patterns. Also, considering the FCS sizing rule, average demands are far from the installed power for all MS scenarios. Highways localized on low variation traffic flow have better relations between sizing and queue length, avoiding early saturation. This improves the FCS load factor.

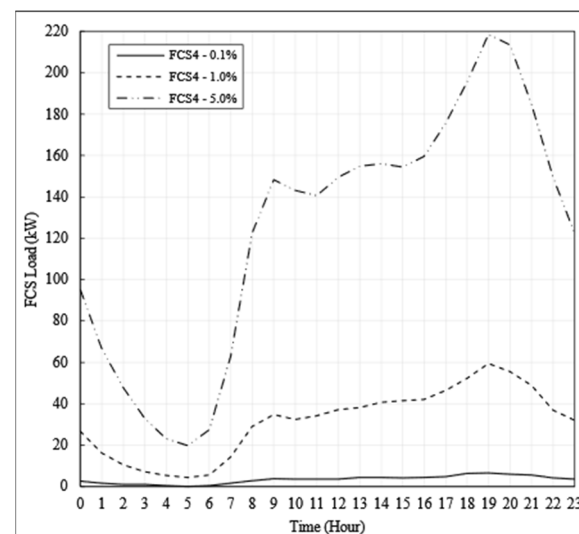


Figure 11. FCS4 load curves for EV market shares of 0.1%, 1%, and 5% of total market vehicles.

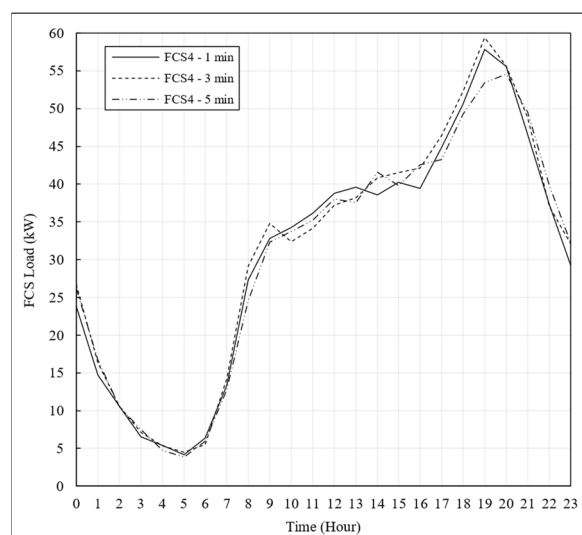
The next sensibility relates to extra-time charger occupancy (δ_{FCS}) and how it influences the queue. Longer times between two consecutive charging events introduce idle periods. The sum of these times generates a cascade of charging event delays, affecting queue conditions.

Varying this parameter on the base case, for FCS4, the highest FCS entry probability, Table 7 returns queue quantiles for 0.85, 0.9, 0.95, and 0.99 at 1, 3, and 5 min of extra-time charger occupancy. Although these three scenarios respect the queue rule and have similar results for 1 and 3 min, the 5 min scenario shows one EV maximum on Q0.9, reaching a 5 EV maximum on Q0.99. Then, the idle time and queue length are directly proportional.

Table 7. Maximum value of highest quantiles for queue length curves for FCS4.

δ_{FCS}	Q0.85	Q0.90	Q0.95	Q0.99
1 min	0	0	1	2
3 min	0	0	1	3
5 min	0	1	2	5

Figure 12 shows the average load curves for these three scenarios. The load curve behavior has a similar pattern considering the same traffic flow simulation. Thus, occupancy rates increase on high-demand hours between 18:00 and 21:00. This period is highly susceptible to queue formation and consecutive charging events, introducing idle times. Longer idle times reduce the average hour load, consequently increasing the queue. It is possible to observe where the load maximum reduces from 60 kW to 55 kW. Technological facilities for autonomous charging coordination and user information campaigns about how to handle the chargers improve these idle times.

**Figure 12.** FCS4 load curves for δ_{FCS} equal to 1, 3, and 5 min.

Other empirical factors are the initial SoC and anxiety range PDFs. Changing α and β influences the maximum and tail forms according to the beta PDF parameters. A variation from the base case was simulated. It created a pessimistic scenario in which the user is carelessly related to the initial SoC and can assume a more apprehensive behavior in front of the minimum SoC.

Table 8 compares the results for both cases, considering FCS4. The new beta function maximum probability for the initial SoC was 0.85 and 0.15 for the anxiety range, updating α and β parameters. For all-day type and highway senses, results to FCS entry probability were duplicated, approximately. Thus, it affects the occupancy rate, resulting in 81% more energy consumed and increasing the queue quantiles, resulting in three EVs on Q0.85 and fifteen EVs on Q0.99, violating the FCS charger rule.

These results demonstrate the sensibility of FCS infrastructures to EV user behavior, mainly in the current market situation. The methodology developed can generate different operational results, being robust mainly for expansion planning studies.

The last methodology analysis is about results stochasticity. Applying the base case parameters, Figure 13 shows the FCS4 stochastic behavior load curve. It simulated ten load curve scenarios (narrow black curves), and it was possible to determine the average load curve (red line) for a random workday in summer. The average curve follows a similar pattern from previous results, with load hours mainly between 7:00 and 21:00 and increasing during the day. Due to the stochastic methodology factors, some simulations

also estimated charging events during the early morning (0:00 until 6:00). Then, based on the stochastic study nature, for applications using this methodology results, it is essential to conduct an uncertainty treatment or an error impact evaluation, e.g., in cases for operation or expansion planning.

Table 8. Results comparison between base and pessimist case related to user behavior parameters for FCS4.

Aspect	Parameter	Base Case	Pessimist Case
SoC	α	28	25
	β	2	5
	$\max(x, f_{Beta})$	0.96	0.85
AR	α	3	5
	β	33	25
	$\max(x, f_{Beta})$	0.06	0.15
FCS Entry Probability	Direct WKDY	0.17	0.36
	Direct WKND	0.18	0.36
	Reverse WKDY	0.37	0.76
	Reverse WKND	0.36	0.77
Energy	2019 FCS Energy	274.58 MWh	496.29 MWh
	Q0.85	0	3
Queue Length	Q0.90	0	5
	Q0.95	1	8
	Q0.99	3	15

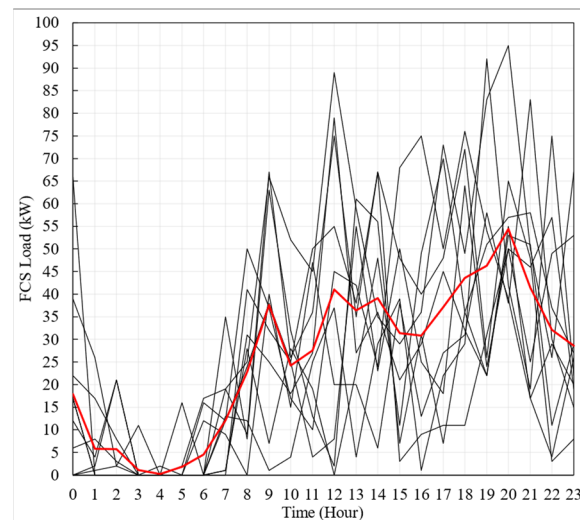


Figure 13. FCS4 stochastic behavior of load curves, considering 1% of EV market share. The black lines are ten load curve scenarios, and the red line represents the scenarios' average load curve.

5. Conclusions

Worldwide mobility technological transitions have significant challenges, mainly related to current user behaviors, anxiety range, EV battery range, and charging times. Public charging infrastructures partially treat these aspects. Focusing on PCI applied to interurban displacements, trips longer than the EV range and without significant travel time impacts are possible by fast-charging station infrastructures.

The literature has been solving FCS highway placing and sizing problems. However, particularities from FCS operation are essential for operation and expansion planning in an infrastructure or power system context. The FCS load curves and queue pattern estimations are the main variables in this planning study, and a lack of methodologies to project these conditions, mainly in a low-available-data environment, was identified.

This article presented a methodology for the FCS operational projection, handling high stochastic parameters. The FCS operational condition is based on two main questions: the relationship between EV users and their vehicles and the relationship between EV users and the highway. The answer to these questions enables us to indicate when the charging event occurs, on a time scale, and how much energy will be used.

The main discussions from the base case and method validation comprise EV infrastructure, EV market, and policy implications.

5.1. Impact on EV Infrastructure

The main supply or service in the EV infrastructure chain is the energy sold to the users. Then, the load curve projection input is elementary for the FCS implementation and operation planning. Obtained from this article's sensibility cases, the FCS occupation rate varies with EV user behaviors, increasing charging probabilities in an SoC-afraid region or without trip planning. Moreover, the FCS localization impacts entry probabilities, charging duration, or both.

The case study showed an FCS localized between two critical points had high probability for a charge event. Otherwise, stations on extreme points or far from cities in influence zones may have low entry probabilities but longer charging events. During the sizing plan step, regions with low entry probabilities needing fewer charger units are only partially valid. This must be regulated by the relation between charging events and charging duration.

Also, FCS load curves on highways follow similar patterns with traffic flow. This must be explored in implementation planning, considering the expected queue on a limited charger resource. In turn, on operation planning, this fact can increase the energy and power demand costs based on time-of-use or real-time energy tariffs models. The recognition of these load patterns allows for better business modeling.

Finally, FCS is deeply impacted by daily and monthly seasonalities. For example, an energy consumption variation between minimum and maximum months of 32% was identified for FCS4 in the base case. In this case, supply contracts must fill this seasonality to a global cost optimization besides the influence on FCS occupancy rates and queue length.

5.2. Impact on EV User Experience and Market

Optimizing the charging process can improve the competitiveness of EVs compared with internal combustion vehicles, mainly in this first EV wave. Guaranteeing good experiences for users can increase market expansion. Based on scenarios obtained from this article, this methodology can improve placing and sizing models, reducing charging durations and increasing infrastructure investments in high-demand regions, influencing queue formation.

Moreover, private and public campaigns could influence current or future EV users for better technology use. The results showed that a smaller initial SoC increases FCS entry probabilities, charging duration, and, consequently, queue length. Also, increasing FCS infrastructures can reduce the user anxiety range, thus better exploring the EV total range. Otherwise, facilities must be implemented for equipment and applications for better process efficiency, reducing, for example, charger idle times.

5.3. Impact on Policies

In the policy environment, FCS load curve estimation methodologies improve the reliability analysis of future EV scenarios. For example, according to sensibility results, infrastructure saturation occurs quickly, according to the EV market share growth. Then, the proposition of FCS policies for new infrastructures can be synchronized with future EV market necessities.

Regarding energy efficiency and Greenhouse Gas Emissions, the FCS load curves indicate future energy deficits and the expected growth for generation, mainly related to

alternative sources or the development of new technologies for energy storage systems, due to the high power demand of FCS with various charging units.

Moreover, the results presented a high relation between FCS load curve shape and traffic patterns. Incentives on energy tariffs, passed on through the charging price by the FCS owner, can introduce new trip strategies for EV users, increasing the low demand factor of FCS and reducing the coincidence load factor with other power system loads once the power limitation for charging events on highways is not a good alternative, considering the user experience.

For power systems, the application of this methodology to project FCS placing and sizing, due to the high-power demand, can modify system expansion policies, including new transmission lines and substations to supply this new load type.

The last results demonstrated operational day stochasticity. Necessarily, all FCS load curves or post-processing models must handle uncertainties due to many EV-related non-controllable parameters. Thus, it is a reliable tool for generating FCS operation conditions according to time step and horizon definitions in data restrictive environments.

The next step is the improvement of this methodology, monitoring and updating stochastic variables' treatment with previous experiences on FCSs already implemented around the world and expanding the problem boundary conditions. The main advances mapped are related to the charging duration, considering minimum-duration connections and the inclusion of EV-type charging load curves, as well as differences between SoC and power demand. Also, an application on FCS energy stochastic optimization related to the FCS load curves is being developed.

Author Contributions: Conceptualization, L.N.F.d.S. and A.d.R.A.; formal analysis, M.B.C. and A.d.R.A.; methodology, L.N.F.d.S., M.B.C. and A.d.R.A.; project administration, A.d.R.A.; algorithms, L.N.F.d.S.; supervision, L.L.P.; validation, L.L.P.; writing—original draft, L.N.F.d.S.; writing—review and editing, L.N.F.d.S., M.B.C., A.d.R.A. and L.L.P. All authors have read and agreed to the published version of the manuscript.

Funding: The authors acknowledge the technical and financial support of Electrical Energy State Company (CEEE-D) and the Equatorial Energy Group (R&D project ANEEL-CEEE/EQUATORIAL/UFSM n° 5000004061), the National Institute of Science and Technology on Distributed Generation Power Systems (INCT-GD), the National Council for Scientific and Technological Development (CNPq—n° 405054/2022-0), Coordination for the Improvement of Higher Education Personnel—Brasil (CAPES—n° 23038.000776/2017-54), the Foundation for Research of the State of Rio Grande do Sul (FAPERGS—n° 17/2551-0000517-1), and the Federal University of Santa Maria (UFSM), Brazilian Institutes.

Data Availability Statement: The original contributions presented in the study are included in the article, further inquiries can be directed to the corresponding author.

Conflicts of Interest: The authors declare no conflicts of interest.

References

1. Das, H.S.; Rahman, M.M.; Li, S.; Tan, C.W. Electric Vehicles Standards, Charging Infrastructure, and Impact on Grid Integration: A Technological Review. *Renew. Sustain. Energy Rev.* **2020**, *120*, 109618. [[CrossRef](#)]
2. IEA. *Global EV Outlook 2022*; IEA Publications: Paris, France, 2022.
3. Hardman, S.; Jenn, A.; Tal, G.; Axsen, J.; Beard, G.; Daina, N.; Figenbaum, E.; Jakobsson, N.; Jochem, P.; Kinnear, N.; et al. A Review of Consumer Preferences of and Interactions with Electric Vehicle Charging Infrastructure. *Transp. Res. Part D Transp. Environ.* **2018**, *62*, 508–523. [[CrossRef](#)]
4. Dong, X.; Mu, Y.; Jia, H.; Wu, J.; Yu, X. Planning of Fast EV Charging Stations on a Round Freeway. *IEEE Trans. Sustain. Energy* **2016**, *7*, 1452–1461. [[CrossRef](#)]
5. Colmenar-Santos, A.; de Palacio, C.; Borge-Diez, D.; Monzón-Alejandro, O. Planning Minimum Interurban Fast Charging Infrastructure for Electric Vehicles: Methodology and Application to Spain. *Energies* **2014**, *7*, 1207–1229. [[CrossRef](#)]
6. Luo, C.; Huang, Y.-F.; Gupta, V. Stochastic Dynamic Pricing for EV Charging Stations With Renewable Integration and Energy Storage. *IEEE Trans. Smart Grid* **2018**, *9*, 1494–1505. [[CrossRef](#)]
7. Motoaki, Y.; Shirik, M.G. Consumer Behavioral Adaption in EV Fast Charging through Pricing. *Energy Policy* **2017**, *108*, 178–183. [[CrossRef](#)]

8. Burnham, A.; Dufek, E.J.; Stephens, T.; Francfort, J.; Michelbacher, C.; Carlson, R.B.; Zhang, J.; Vijayagopal, R.; Dias, F.; Mohanpurkar, M.; et al. Enabling Fast Charging—Infrastructure and Economic Considerations. *J. Power Sources* **2017**, *367*, 237–249. [[CrossRef](#)]
9. Gusrialdi, A.; Qu, Z.; Simaan, M.A. Scheduling and Cooperative Control of Electric Vehicles' Charging at Highway Service Stations. In Proceedings of the 53rd IEEE Conference on Decision and Control, Los Angeles, CA, USA, 15–17 December 2014; IEEE: New York, NY, USA, 2014; pp. 6465–6471.
10. Zarazua de Rubens, G.; Noel, L.; Kester, J.; Sovacool, B.K. The Market Case for Electric Mobility: Investigating Electric Vehicle Business Models for Mass Adoption. *Energy* **2020**, *194*, 116841. [[CrossRef](#)]
11. Napoli, G.; Polimeni, A.; Micari, S.; Andaloro, L.; Antonucci, V. Optimal Allocation of Electric Vehicle Charging Stations in a Highway Network: Part 1. Methodology and Test Application. *J. Energy Storage* **2020**, *27*, 101102. [[CrossRef](#)]
12. Dong, X.; Yuan, K.; Song, Y.; Mu, Y.; Jia, H. A Load Forecast Method for Fast Charging Stations of Electric Vehicles on the Freeway Considering the Information Interaction. *Energy Procedia* **2017**, *142*, 2171–2176. [[CrossRef](#)]
13. Korolko, N.; Sahinoglu, Z.; Nikovski, D. Modeling and Forecasting Self-Similar Power Load Due to EV Fast Chargers. *IEEE Trans. Smart Grid* **2016**, *7*, 1620–1629. [[CrossRef](#)]
14. Arias, M.B.; Bae, S. Electric Vehicle Charging Demand Forecasting Model Based on Big Data Technologies. *Appl. Energy* **2016**, *183*, 327–339. [[CrossRef](#)]
15. Savari, G.F.; Krishnasamy, V.; Sathik, J.; Ali, Z.M.; Abdel Aleem, S.H.E. Internet of Things Based Real-Time Electric Vehicle Load Forecasting and Charging Station Recommendation. *ISA Trans.* **2020**, *97*, 431–447. [[CrossRef](#)] [[PubMed](#)]
16. Daneshzand, F.; Coker, P.; Potter, B.; Smith, S. EV smart charging: How tariff selection influences grid stress and carbon reduction. *Appl. Energy* **2023**, *348*, 121482. [[CrossRef](#)]
17. Silva, L.; Abaide, A.; Sausen, J.; Paixão, J.; Correa, C. Proposal of a Load Curve modeling applied to Highway EV Fast Charging Stations. In Proceedings of the 2021 56th International Universities Power Engineering Conference (UPEC), Middlesbrough, UK, 31 August–3 September 2021; IEEE: New York, NY, USA, 2021. [[CrossRef](#)]
18. Domínguez-Navarro, J.A.; Dufo-López, R.; Yusta-Loyo, J.M.; Artal-Sevil, J.S.; Bernal-Agustín, J.L. Design of an Electric Vehicle Fast-Charging Station with Integration of Renewable Energy and Storage Systems. *Int. J. Electr. Power Energy Syst.* **2019**, *105*, 46–58. [[CrossRef](#)]
19. Bae, S.; Kwasinski, A. Spatial and Temporal Model of Electric Vehicle Charging Demand. *IEEE Trans. Smart Grid* **2012**, *3*, 394–403. [[CrossRef](#)]
20. del Razo, V.; Jacobsen, H.-A. Smart Charging Schedules for Highway Travel With Electric Vehicles. *IEEE Trans. Transp. Electrif.* **2016**, *2*, 160–173. [[CrossRef](#)]
21. Yuan, K.; Song, Y.; Shao, Y.; Sun, C.; Wu, Z. A Charging Strategy with the Price Stimulus Considering the Queue of Charging Station and EV Fast Charging Demand. *Energy Procedia* **2018**, *145*, 400–405. [[CrossRef](#)]
22. Paatero, J.V.; Lund, P.D. A Model for Generating Household Electricity Load Profiles. *Int. J. Energy Res.* **2006**, *30*, 273–290. [[CrossRef](#)]
23. Armstrong, M.M.; Swinton, M.C.; Ribberink, H.; Beausoleil-Morrison, I.; Millette, J. Synthetically Derived Profiles for Representing Occupant-Driven Electric Loads in Canadian Housing. *J. Build. Perform. Simul.* **2009**, *2*, 15–30. [[CrossRef](#)]
24. Quiros-Tortos, J.; Ochoa, L.F.; Lees, B. A Statistical Analysis of EV Charging Behavior in the UK. In Proceedings of the 2015 IEEE PES Innovative Smart Grid Technologies Latin America (ISGT LATAM), Montevideo, Uruguay, 5–7 October 2015; IEEE: New York, NY, USA, 2015; pp. 445–449.
25. Hardinghaus, M.; Blümel, H.; Seidel, C. Charging Infrastructure Implementation for EVs—The Case of Berlin. *Transp. Res. Procedia* **2016**, *14*, 2594–2603. [[CrossRef](#)]
26. Langbroek, J.H.M.; Franklin, J.P.; Susilo, Y.O. When Do You Charge Your Electric Vehicle? A Stated Adaptation Approach. *Energy Policy* **2017**, *108*, 565–573. [[CrossRef](#)]
27. Gnann, T.; Funke, S.; Jakobsson, N.; Plötz, P.; Sprei, F.; Bennehag, A. Fast Charging Infrastructure for Electric Vehicles: Today's Situation and Future Needs. *Transp. Res. Part D Transp. Environ.* **2018**, *62*, 314–329. [[CrossRef](#)]
28. Rominger, J.; Farkas, C. Public Charging Infrastructure in Japan—A Stochastic Modelling Analysis. *Int. J. Electr. Power Energy Syst.* **2017**, *90*, 134–146. [[CrossRef](#)]
29. DNIT Plano Nacional de Contagem de Tráfego. Available online: <http://servicos.dnit.gov.br/dadospnt/ContagemContinua> (accessed on 25 March 2022).

Disclaimer/Publisher's Note: The statements, opinions and data contained in all publications are solely those of the individual author(s) and contributor(s) and not of MDPI and/or the editor(s). MDPI and/or the editor(s) disclaim responsibility for any injury to people or property resulting from any ideas, methods, instructions or products referred to in the content.